Published in final edited form as:
Bone. 2014 September ; 66: 56–61. doi:10.1016/j.bone.2014.06.004.

Magnetic resonance imaging assessed cortical porosity is highly correlated with μCT porosity

Won C Bae[1,4], **Shantanu Patil**[2], **Reni Biswas**[1], **Shihong Li**[1,3], **Eric Y Chang**[4,1], **Sheronda Statum**[1,4], **Darryl D D'Lima**[2], **Christine B Chung**[4,1], and **Jiang Du**[1,4]

[1]Department of Radiology, University of California, San Diego, CA

[2]Shiley Center for Orthopaedic Research & Education, Scripps Clinic, La Jolla, CA

[3]Department of Radiology, Hua Dong Hospital, Fudan University, Shanghai, P.R. China

[4]Department of Radiology, VA San Diego Healthcare System, La Jolla, CA

Abstract

Cortical bone is typically regarded as “MR invisible” with conventional clinical magnetic resonance imaging (MRI) pulse sequences. However, recent studies have demonstrated that free water in the microscopic pores of cortical bone has a short T2* but a relatively long T2, and may be detectable with conventional clinical spin echo (SE) or fast spin echo (FSE) sequences. In this study we describe the use of a conventional two-dimensional (2D) FSE sequence to assess cortical bone microstructure and measure cortical porosity using a clinical 3T scanner. Twelve cadaveric human cortical bone samples were studied with MRI and micro computed tomography (μCT) (downsampled to the same spatial resolution). Preliminary results show that FSE-determined porosity is highly correlated ($R^2 = 0.83$; $P < 0.0001$) with μCT porosity. Bland Altman analysis suggested a good agreement between FSE and μCT with tight limit of agreement at around 3%. There is also a small bias of -2% for the FSE data, which suggested that the FSE approach slightly underestimated μCT porosity. The results demonstrate that cortical porosity can be directly assessed using conventional clinical FSE sequences. The clinical feasibility of this approach was also demonstrated on six healthy volunteers using 2D FSE sequences as well as 2D ultrashort echo time (UTE) sequences with a minimal echo time (TE) of 8 μs, which provide high contrast imaging of cortical bone in vivo.

Keywords

Fast spin echo; UTE; porosity; cortical bone; μCT

Introduction

Cortical bone is a composite material containing approximately 20-25% water by volume [1-3]. Bone water occurs at various locations and in different binding states. In normal bone the majority of bone water is loosely bound to the organic matrix (collagen and cement

Corresponding Author: Jiang Du, Ph.D., jiangdu@ucsd.edu, University of California, San Diego, Department of Radiology, 200 West Arbor Drive, San Diego, CA 92103-8226, Phone (619) 471-0519, Fax (619) 471-0503.

substance), with a minor fraction tightly bound to bone mineral [4-6]. There is also a significant amount of free water residing in the microscopic pores of the Haversian and the lacunocanalicular systems, responsible for nutrient diffusion and contributing to viscoelastic properties of the material [1, 7]. Pore diameters range from tens to hundreds of micrometers in the Haversian canals and several micrometers in the lacunae down to submicrometer dimensions in the canaliculi [7-9].

Both loosely and tightly bound water have very short T2 and cannot be assessed by conventional magnetic resonance imaging (MRI) techniques [5, 10-14]. Free water residing in the pores have short T2* (e.g., 1-6 ms at 0.66 T [5], 2-3 ms at 3 T [6, 12], ~1 ms at 4.7 T [4]) but relatively long T2 (1 ms to 2000 ms at 0.66 T [10], 1 ms to 1000 ms at 4.7 T [4]), and can potentially be imaged with conventional spin echo (SE) or fast spin echo (FSE) sequences, providing a way for non-invasive radiation-free assessment of cortical porosity using MRI techniques [4-6]. While it is challenging to assess small pores in the lacunocanalicular systems, it is technically feasible to directly image water residing in the big Haversian canals with pore size on the order of hundreds of micrometers [12, 13]. Bell et al. have shown that there are a group of canals termed “giant' canals with pore diameters > 385 μm, which contribute to over 27% of the porosity despite comprising only approximately 1% of the canal population [14-16]. These “giant” canals have a markedly negative influence on the ability of the cortical bone shell to withstand stresses associated with a fall, and lead to much increased risk for osteoporotic fracture [14-16]. FSE assessment of free water in these “giant” canals as well as smaller canals may allow clinically relevant assessment of cortical porosity, which has been shown to have a dramatic impact on the mechanical properties of cortical bone [14]. In this study, we aimed to investigate bone water imaging with clinical FSE sequences, and to correlate the structure seen with FSE imaging with that seen with micro computed tomography (μCT) imaging. Clinical feasibility of FSE imaging of cortical bone in vivo was also demonstrated on healthy volunteers. Ultrashort echo time (UTE) imaging was performed on the volunteers for comparison.

Materials and Methods

Bone Samples Preparation

Cadaveric human tibial midshaft samples (centered at approximately 50% of tibial length proximal to the lateral malleolus) from twelve donors (8 males, 4 females; age range 32-90 years, 62 ± 16 years old, mean ± standard deviation) were harvested from cadaveric leg specimens obtained from the University of California, San Diego (UCSD) morgue, and were cleared of external muscle and soft tissue. Bone marrow was removed with a scalpel. Cross-sectional cortical bone segments with an approximate thickness of 3 to 5 mm were cut under constant saline irrigation using a low-speed precision circular diamond-edge saw (Isomet 1000, Buehler, Lake Bluff, IL). Individual samples were wrapped in saline-wet gauze and frozen at -70 °C in an ultralow freezer (Bio-Freezer; Forma Scientific, Marietta, OH, USA). The samples were allowed to thaw in phosphate buffered saline (PBS) solution for 24 hours at 4 °C prior to MR imaging. After this, samples were imaged with μCT to assess their bone structure. All MRI and μCT studies were performed within Institutional Review Board guidelines.

MRI of Bone Samples

Clinical 2D FSE sequences were used to image free water in cortical bone on a 3T General Electric whole-body scanner (GE Healthcare Technologies, Milwaukee, WI). The system had gradients capable of a slew rate of 150 T/m/s and an amplitude of 40 mT/m on each axis. Each bone sample was placed in a 30 ml syringe filled with Fomblin perfluoropolyether (Solvay SA, Brussels, Belgium) during MR imaging to maintain hydration and minimize susceptibility effects at air-bone junctions. Typical FSE imaging parameters included: field of view (FOV) = 4 cm, slice thickness = 0.5 mm, reconstruction matrix = 512×512, sampling bandwidth = 62.5 kHz, sinc pulses (duration = 3.2 ms, spectral bandwidth = 2 kHz) for signal excitation and refocusing, TR = 4000 ms, effective TE = 18.7 ms, echo train length (ETL) = 4, total scan time = 9 minutes. A 2-inch birdcage coil was used for signal excitation and reception.

μCT of Bone Samples

Bone samples were imaged using a Skyscan 1076 (Bruker microCT, Kontich, Belgium) μCT scanner with the following parameters: 1 mm aluminum filter, 90 kV, 112 μA, rotation step = 1 degree, voxel size = 36.24 μm isotropic, exposure time = 90 ms per rotation, scan time = 30 minutes. Tomographic images were reconstructed using Skyscan NRecon software (version 1.6.8.0) using Feldkamp cone-beam backprojection algorithm with noise and ring-artifact reduction.

Image Registration

MRI FSE and μCT datasets were first manually scaled to identical voxel size and roughly aligned using ImageJ software [17], and then automatically registered using FLIRT (Functional MRI of the Brain's Linear Image Registration Tool) software using 6 parameter rigid body model and correlation ratio as the cost function [18, 19]. After registration, since MR data had thicker slice thickness, μCT images were averaged in multiple stacks to achieve the same thickness as the MR images.

Cortical Porosity Calculation

On both MRI and μCT datasets, 3 to 5 slices (anatomically axial) from the middle of the dataset were selected for analysis. Middle slices were used to avoid partial volume artifacts often seen on slices near the ends of the sample. Regions of interest (ROI) representing the cortical shell were drawn on μCT and applied to both MR and μCT datasets (Figure 2DE). For thresholding, MR data was first inverted (to make bone areas high signal intensity and pores low signal intensity), while μCT data was processed without inverting. Otsu's methods were used to automatically binarize each image, based on the histogram of signal intensities and minimization of intra-class variation [20]. On binarized images where white represented bone and black represented pores, apparent porosity was determined as the ratio of pore areas divided by the ROI area.

In Vivo MRI of Cortical Bone

The 2D FSE sequence was also used to image the mid-diaphyseal tibia in six healthy volunteers (all males, ranging in age from 34 to 68 years, average age of 52). Written

informed consent approved by our Institutional Review Board was obtained prior to their participation in this study. Imaging parameters were similar to those used in the cadaveric study, except a thicker slice of 0.7 mm, shorter TR of 3 sec, and shorter total scan time of 6 min. A 2.5 cm receive-only surface coil was used for signal reception and the body coil was used for signal excitation. For comparison, a 2D ultrashort echo time (UTE) imaging sequence with a minimal nominal TE of 8 μs was employed to image cortical bone in vivo [21]. An adiabatic inversion recovery preparation pulse was employed to suppress signal from long T2 muscle and marrow fat, providing high contrast imaging of cortical bone [11]. Typical UTE and IR-UTE imaging parameters were: FOV = 4 cm, slice thickness = 3 mm, bandwidth = 62.5 kHz, sampling points = 137, reconstruction matrix = 512×512 (zero-filled interpolation), TR = 300 ms, TE = 8 μs, TI = 120 ms (for IR-UTE imaging only), total scan time = 5 minutes.

Statistical Analysis

Agreement between porosity values determined using MRI and μCT was evaluated using a number of methods. Pearson correlation and intraclass correlation analyses were performed. In addition, Bland-Altman analysis was performed to determine bias and limit of agreement. MRI and μCT data analyses were performed by two observers (WCB and RB) independently. Inter-observer intraclass correlation coefficient was calculated.

Results

Bone water in large pores and canals can be imaged directly in vitro using conventional multi-slice 2D FSE sequences, as shown in Figure 1. Cortical bone structure is well depicted in both the axial and coronal planes. The high signals are consistent with free water residing in the Haversian systems which has relatively long T2 and can be detected by regular FSE sequences.

Figure 2 shows selected 2D FSE images and μCT images of four representative cortical bone samples. There is a high morphological correlation between these two imaging techniques: the high signal in FSE images correlates well with the signal void in μCT images. More porous bone shows increased high signal in FSE images as well as increased signal void in μCT images. These results suggest that 2D FSE imaging is able to detect cortical pore structure.

More details on image registration and cortical porosity calculation are shown in Figure 3. In this figure a representative bone sample was shown in the axial plane with registered FSE and μCT images together with the difference image, which suggests that excellent rigid body registration was achieved. Regions of interest representing the cortical shell (yellow line, DEF) were drawn, and thresholded. Porosity determined from FSE (D) and μCT (E) were similar, and showed good overlap on the difference image (F), where white, red, and blue areas indicate areas of overlap, μCT-only, and FSE-only, respectively.

Cortical porosity derived from MRI and μCT data were analyzed by two observers independently, with a significant inter-observer intraclass correlation coefficient of 0.84. Figure 4 shows linear regression (A) and Bland-Altman analysis (B) between porosity

assessed by μCT imaging and 2D FSE imaging. There is a high correlation between these two imaging modalities ($R^2 = 0.83$; $P < 0.0001$), suggesting that clinical 2D FSE imaging can reliably assess cortical porosity. Bland-Altman plot shows the difference between porosity obtained from MRI and μCT versus the porosity determined on μCT as the reference. Bland Altman analysis suggested a good agreement between FSE and μCT, with a small bias of -2% for the FSE data, which meant that the FSE approach slightly underestimated μCT porosity. The limit of agreement was also tight, at around 3%.

Our results also show that bone water in large pores can be imaged in vivo using conventional 2D multi-slice FSE sequences (Figure 5). The use of small surface coils allows high spatial resolution imaging of cortical bone in vivo with voxel sizes down to 78×78×700 μm^3. Regular UTE sequences provide images of both bound water (uniform background signal in the tibial cortex) and free water (fine structures in the tibial cortex), but with limited contrast due to the high signal from surrounding muscle and fat which have much longer T2s and higher proton densities. The IR-UTE sequence provides selective imaging of water bound to the organic matrix (highlighted as uniform background signal in the tibial cortex), with free water being inverted and nulled by the adiabatic inversion recovery preparation pulse. Compared to the younger volunteer, the older volunteer shows increased structure in cortical bone with the FSE sequence, consistent with increased cortical porosity with aging in healthy volunteers.

Discussion

Osteoporosis (OP) is defined as a systemic skeletal disorder characterized by low bone mass and microarchitectural deterioration of bone tissue, resulting in thinning and increased cortical porosity, bone fragility and fracture risk. Recent clinical investigations indicate that the evaluation of bone mineral density (BMD) by dual-energy x-ray absorptiometry (DXA) has limitations in assessing fracture risk and monitoring the response to therapy [22-24]. There is progressively increased interest in new non-invasive and/or non-destructive techniques, including high resolution CT and MRI which are able to provide structural information about the pathophysiology of bone fragility. Microarchitecture is considered the key to bone quality [25]. The trabecular bone microarchitecture can be assessed by high resolution CT (hrCT), high resolution peripheral quantitative CT (HRpQCT), μCT, high resolution MRI (hrMRI) and micro MRI (μMRI) [26-28]. The cortical bone microarchitecture can be assessed by μCT and HRpQCT [28-32]. hrCT, HRpQCT, and hrMRI are generally applicable in vivo, while μCT can only be used in vitro. The recent development of HRpQCT with spatial resolution down to 82 μm has allowed in-vivo assessment of bone porosity in healthy volunteers and OP patients. HRpQCT assessed age-related differences in cortical porosity are more pronounced than differences in standard cortical metrics [30]. HRpQCT measured cortical porosity is highly correlated with μCT porosity ($R^2 = 0.80$) [29]. Preliminary results have also shown a high correlation between cortical porosity and biomechanical assessment [29-32].

The capability of non-invasively assess cortical porosity is of high importance for the evaluation of bone quality with relevance to diagnosis, prognosis, and sensitive monitoring of drug therapy outcomes. Bone loss involves thinning of the cortex and an increase in

intracortical porosity which typically ranges from 5% to 39% in the human femoral neck [33]. Cortical bone strength, fracture toughness, stiffness and elastic modulus are all affected by the levels of cortical porosity. McCalden et al. showed that porosity changes in the femur account for 76% of the variance in age-related decline in strength. Increased porosity decreases elasticity and fracture toughness [34]. A 4% rise in cortical porosity increases crack propagation through bone by 84% [35]. An increase in porosity from 4% to 10% more than halves the peak stress that can be tolerated by bone before fracture [36]. Fracture toughness is affected by changes in porosity but is independent of BMD [36].

However, x-ray based techniques, including hrCT and HRpQCT, subject the patient to ionizing radiation and is not suitable for repeated measurements over the long term evolution and treatment of OP, or for use in children or pregnant women. MRI-based techniques have the advantages of assessing trabecular bone microarchitecture free from ionizing radiation [1, 37]. Recent research by Ladinsky et al. demonstrated that trabecular structure at the distal radius quantified with the hrMRI based virtual bone biopsy explained a significant portion of the variation in total spinal deformity burden in postmenopausal women independent of areal BMD [38]. In this study, we further demonstrate that hrMRI can assess cortical porosity. Previous NMR spectroscopy studies have shown that free water residing in the microscopic pores of cortical bone (Haversian canals, super-osteons or remodeling clusters in the cortex) can have relatively long T2 values of 100 ms or longer [5, 10]. This portion of bone water can be imaged with conventional clinical SE or FSE sequences with TEs of around 10 ms [5,6,12,13]. The relative large pore size, especially the super-osteons or “giant canals” helps high resolution imaging of free water. Our earlier studies demonstrate that pore water has relatively long T2 but a short T2*, and cannot be readily imaged with clinical gradient echo sequences [12,13]. UTE sequences can detect signal from both free water in the pores and water loosely bound to the organic matrix [12, 39-41].

As mentioned earlier, the 2D FSE imaging sequence targets signal from free water in big pores. Haversian canal diameters can vary greatly within a single bone due to the formation of Haversian systems by the refilling of resorption spaces, as well as the simultaneous presence of systems at various states in the remodeling process. Current literatures suggest the size of resorption spaces in human bone to be on the order of 200 to 300 microns [42]. Thomas et al. investigated the relative contributions of pore size and pore density (number of pores per mm^2) to porosity in the midshaft of the human femur and found increase in pore area, not pore density, is the main determinant in the development of porosity in human cortical bone [43].

Remodeling involves the close coordination of osteoblasts and osteoclasts in what is known as the basic multicellular unit (BMU), and it creates secondary osteons [44]. The BMU in bone is conventionally described to have cylindrical geometry, which is highly idealized. A variety of BMU related irregular resorption space forms exists, including localized dilations of existing canals, branched and double-ended cutting cones and irregular interconnected spaces [9, 42, 45]. As early as 1958 Cohen and Harris investigated the 3D anatomy of Haversian systems and found the existence of irregular and highly interconnected resorption spaces in canine femoral bone [45]. Johnson studied morphological analysis of pathology and described canals with eccentric and variable patterns of resorption in human cortical bone [42].

Remodeling may have a higher level of organization which is above that of the single osteon. Bell et al. proposed “super-osteon” to describe the collective structure of spatially and temporally clustered secondary osteons [15]. They reported “composite” osteons which are comprised of multiple incomplete packets of new bone and associated with enlarged osteonal canals [16]. They further suggested that a breakdown in the control of resorption depth led to the merger of adjacent canals into giant canals. Employing high resolution 3D μCT, Cooper et al. found that resorption spaces can frequently intersect with numerous existing canals along their length as well as progressive trabecularization of the cortex through the coalescence of ever larger canals [9]. They found enlarged canals frequently spanned in excess of 7 mm [9], although a mean osteon length (defined as distance between canal intersections) has been reported to be 2.5 mm for the human femoral cortex [46]. Spatial clustering of remodeling osteons is linked with increased fracture risk. Interestingly no resorption spaces were found in females 81 years and older due to extensive trabecularization in cortices [9].

The current study indicates that high resolution FSE sequences can directly assess cortical porosity in a clinical setting. Cortical porosity can be estimated based on high resolution MR imaging of free water residing in the fine structures of cortical bone, which requires a high spatial resolution of around 100 μm or better for optimal depiction. A small coil in close proximity to bone is required for optimal imaging [12]. Considering the longitudinal structure of Haversian canals, axial imaging with thick slices is one option to improve signal to noise ratio (SNR) for clinical assessment of cortical bone structure. In the in vivo application, we employed a 2.5 cm surface coil for signal reception, which together with a relatively thicker slice of 0.7 mm allows high resolution imaging of cortical bone with enough SNR support. Further optimization of the imaging parameters, including slightly reduced slice resolution to gain higher SNR, reduced in-plane resolution to target larger pores, bigger coils with slightly lower SNR efficiency but more spatial coverage, may further improve the evaluation of cortical bone in vivo. Quantitative assessment of free water content with UTE techniques is another way to assess cortical porosity [47-49]. The accuracy of this approach remains to be demonstrated and comparison of this approach with SE or FSE assessment of cortical porosity as well as μCT porosity will be performed in future studies.

Conclusion

Cortical bone microstructure can be assessed with a FSE technique utilizing a clinical 3T scanner. This technique strongly correlates with cortical porosity measured from downsampled μCT images of cadavers. We have also demonstrated the clinical feasibility of this technique in volunteers.

Acknowledgments

The authors thank grants support from GE Healthcare, 1R01 AR062581-01A1 and 1R21 AR063894-01A1.

References

1. Wehrli FW, Song HK, Saha PK, Wright AC. Quantitative MRI for the assessment of bone structure and function. NMR in Biomed. 2006; 19:731–764.

2. Lees S. A mixed pacing model for bone collagen. Calcif Tissue Int. 1981; 33:591–602. [PubMed: 6799171]
3. Yeni YN, Brown CU, Norman TL. Influence of bone composition and apparent density on fracture toughness of the human femur and tibia. Bone. 1998; 22:79–84. [PubMed: 9437517]
4. Horch RA, Nyman JS, Gochberg DF, Dortch RD, Does MD. Characterization of 1H NMR signal in human cortical bone for magnetization resonance imaging. Magn Reson Med. 2010; 64:680–687. [PubMed: 20806375]
5. Nyman JS, Ni Q, Nicolella DP, Wang X. Measurements of mobile and bound water by nuclear magnetic resonance correlate with mechanical properties of bone. Bone. 2008; 42:193–199. [PubMed: 17964874]
6. Biswas R, Bae WC, Diaz E, Masuda K, Chung CB, Bydder GM, Du J. Ultrashort echo time (UTE) imaging with bicomponent analysis: bound and free water evaluation of bovine cortical bone subject to sequential drying. Bone. 2012; 50:749–755. [PubMed: 22178540]
7. Cowin SC. Bone poroelasticity. J Biomechanics. 1999; 32:217–238.
8. Beddoe AH. Measurements of the microscopic structure of cortical bone. Phys Med Biol. 1977; 22:298–304. [PubMed: 857264]
9. Cooper DM, Thomas CD, Clement JG, Hallgrimsson B. Three-dimensional microcomputed tomography imaging of basic multicellular unit-related resorption spaces in human cortical bone. Anat Rec A Discov Mol Cell Evol Biol. 2006; 288:806–816. [PubMed: 16761291]
10. Ni Q, Nyman JS, Wang X, De Los Santos A, Nicolella DP. Assessment of water distribution changes in human cortical bone by nuclear magnetic resonance. Meas Sci Technol. 2007; 18:715–723.
11. Du J, Carl M, Bydder M, Takahashi A, Chung CB, Bydder GM. Qualitative and quantitative ultrashort echo time (UTE) imaging of cortical bone. J Magn Reson. 2010; 207:304–311. [PubMed: 20980179]
12. Du J, Hermida JC, Diaz E, Corbeil J, Znamirowski R, D'Lima DD, Bydder GM. Assessment of cortical bone with clinical and ultrashort echo time sequences. Magn Reson Med. 2013; 70:697–704.
13. Du, J.; Bae, WC.; Bydder, M.; Carl, M.; Takahashi, A.; Chung, CB.; Bydder, GM. Assessment of cortical bone structure with FSE, 2D and 3D UTE sequences. International Society for Magnetic Resonance in Medicine (ISMRM) Workshop: Advances in Musculoskeletal Magnetic Resonance Imaging; San Francisco, CA, USA,. 14-17 February, 2009;
14. Bell KL, Loveridge N, Power J, Garrahan N, Meggitt BF, Reeve J. Regional differences in cortical porosity in the fractured femoral neck. Bone. 1999; 24:57–64. [PubMed: 9916785]
15. Bell KL, Loveridge N, Reeve J, Thomas CD, Feik SA, Clement JG. Super-osteons (remodeling clusters) in the cortex of the femoral shaft: influence of age and gender. Anat Rec. 2001; 264:378–386. [PubMed: 11745093]
16. Bell KL, Loveridge N, Jordan GR, Power J, Constant CR, Reeve J. A novel mechanism for induction of increased cortical porosity in cases of intracapsular hip fracture. Bone. 2000; 27:297–304. [PubMed: 10913926]
17. Schneider CA, Rasband WS, Eliceiri KW. NIH Image to ImageJ: 25 years of image analysis. Nature Methods. 2012; 9:671–675. [PubMed: 22930834]
18. Jenkinson M, Smith SM. A global optimisation method for robust affine registration of brain images. Medical Image Analysis. 2001; 5:143–156. [PubMed: 11516708]
19. Jenkinson M, Bannister PR, Brady JM, Smith SM. Improved optimisation for the robust and accurate linear registration and motion correction of brain images. NeuroImage. 2002; 17:825–841. [PubMed: 12377157]
20. Otsu N. A threshold selection method from gray-level histograms. IEEE Trans Sys Man, Cyber. 1979; 9:62–66.
21. Du J, Hamilton G, Takahashi A, Bydder M, Chung CB. Ultrashort TE spectroscopic imaging (UTESI) of cortical bone. Magn Reson Med. 2007; 58:1001–1009. [PubMed: 17969110]
22. Cummings SR. How drugs decrease fracture risk: lessons from trials. J Musculoskeletal Neuronal Interact. 2002; 2:198–200.

23. Delmas P, Seeman E. Changes in bone mineral density explain little of the reduction in vertebral or nonvertebral fracture risk with anti-resorptive therapy. Bone. 2004; 34:599–604. [PubMed: 15050889]
24. Watts NB, Geusens P, Barton IP, Felsenberg D. Relationship between changes in BMD and nonvertibral fracture incidence associated with risedronate: reduction in risk of nonvertibral fracture is not related to change in BMD. J Bone Miner Res. 2005; 20:2097–2104. [PubMed: 16294263]
25. Brandi ML. Microarchitecture, the key to bone quality. Rheumatology. 2009; 48:3–8.
26. Genant HK, Engelke K, Prevrhal S. Advanced CT bone imaging in osteoporosis. Rheumatology. 2008; 47:9–16.
27. Liu XS, Cohen A, Shane E, Stein E, Rogers H, Kokolus SL, Yin PT, McMahon DJ, Lappe JM, Recker RR, Guo XE. Individual trabeculae segmentation (ITS)-based morphological analysis of high-resolution peripheral quantitative computed tomography images detect abnormal trabecular plate and rod microarchitecture in premenopausal women with idiopathic osteoporosis. J Bone Miner Res. 2010; 25:1496–1505. [PubMed: 20200967]
28. Krug R, Burghardt AJ, Majumdar S, Link TM. High-resolution imaging techniques for the assessment of osteoporosis. Radiol Clin North Am. 2010; 48:601–621. [PubMed: 20609895]
29. Nishiyama KK, Macdonald HM, Hanley DA, Boyd SK. Women with previous fragility fractures can be classified based on bone microarchitecture and finite element analysis measured with HR-pQCT. Osteoporosis Int. 2013; 24:1733–1740.
30. Burghardt AJ, Kazakia GJ, Ramachandran S, Link TM, Majumdar S. Age and gender related differences in the geometric properties and biomechanical significance of intra-cortical porosity in the distal radius and tibia. J Bone Miner Res. 2010; 25:983–993. [PubMed: 19888900]
31. Burghardt AJ, Buie HR, Laib A, Majumdar S, Boyd SK. Reproducibility of direct quantitative measures of cortical bone microarchitecture of the distal radius and tibia by HR-pQCT. Bone. 2010; 47:519–528. [PubMed: 20561906]
32. Burghardt AJ, Pialat JB, Kazakia GJ, Boutroy S, Engelke K, Patsch JM, Valentinitsch A, Liu D, Szabo E, Bogado CE, Zanchetta MB, McKay HA, Shane E, Boyd SK, Bouxsein ML, Chapurlat R, Khosla S, Majumdar S. Multicenter precision of cortical and trabecular bone quality measures assessed by high-resolution peripheral quantitative computed tomography. J Bone Miner Res. 2013; 28:524–536. [PubMed: 23074145]
33. Bousson V, Peyrin F, Bergot C, Hausard M, Sautet A, Laredo JD. Cortical bone in the human femoral neck: three-dimensional appearance and porosity using synchrotron radiation. J Bone Miner Res. 2004; 19:794–801. [PubMed: 15068503]
34. McCalden RW, McGeough JA, Barker MB, Court-Brown CM. Age-related changes in the tensile properties of cortical bone: the relative importance of changes in porosity, mineralization and microstructure. J Bone Joint Surg Am. 1993; 75:1193–1205. [PubMed: 8354678]
35. Diab T, Vashishth D. Effects of damage morphology on cortical bone fragility. Bone. 2005; 37:96–102. [PubMed: 15897021]
36. Martin, RB.; Burr, DB. The microscopic structure of bone In: Structure, function, and adaptation of compact bone. New York, NY, USA: Raven Press; 1989.
37. Takahashi M, Wehrli FW, Hilaire L, Zemel B, Hwang SN. In vivo NMR microscopy allows short-term serial assessment of multiple skeletal implications of corticosteroid exposure. Proc Natl Acad Sci USA. 2002; 99:4574–4579. [PubMed: 11904367]
38. Ladinsky GA, Vasilic B, Popescu AM, Wald M, Zemel BS, Snyder PJ, Loh L, Song HK, Saha PK, Wright AC, Wehrli FW. Trabecular Structure Quantified With the MRI-Based Virtual Bone Biopsy in Postmenopausal Women Contributes to Vertebral Deformity Burden Independent of Areal Vertebral BMD. J Bone Miner Res. 2008; 23:64–74. [PubMed: 17784842]
39. Diaz E, Chung CB, Bae WC, Statum S, Znamirowski R, Bydder GM, Du J. Ultrashort echo time spectroscopic imaging (UTESI): an efficient method for quantifying bound and free water. NMR Biomed. 2012; 25:161–168. [PubMed: 21766381]
40. Du J, Diaz E, Carl M, Bae WC, Chung CB, Bydder GM. Ultrashort echo time imaging with bicomponent analysis. Magn Reson Med. 2012; 67:645–649. [PubMed: 22034242]

41. Bae WC, Chen PC, Chung CB, Masuda K, D'Lima D, Du J. Quantitative ultrashort echo time (UTE) MRI of human cortical bone: correlation with porosity and biomechanical properties. J Bone Miner Res. 2012; 27:848–857. [PubMed: 22190232]

42. Jaworski ZF, Meunier P, Frost HM. Observations on two types of resorption cavities in human lamellar cortical bone. Clin Orthop. 1972; 83:279–285. Johnson LC 1964. [PubMed: 5014823]

43. Thomas CDL, Feik SA, Clement JG. Increase in pore area, and not pore density, is the main determinant in the development of porosity in human cortical bone. J Anat. 2006; 209:219–230. [PubMed: 16879600]

44. Frost HM. Relation between bone tissue and cell population dynamics, histology and tetracycline labeling. Clin Orthop. 1966; 49:65–75. [PubMed: 5962624]

45. Cohen J, Harris W. The three-dimensional anatomy of haversian systems. J Bone Joint Surg Am. 1958; 40:419–434. [PubMed: 13539066]

46. Beddoe AH. Measurements of the microscopic structure of cortical bone. Phys Med Biol. 1977; 22:298–304. [PubMed: 857264]

47. Du J, Bydder GM. Qualitative and quantitative ultrashort-TE MRI of cortical bone. NMR Biomed. 2013; 26:489–506. [PubMed: 23280581]

48. Horch RA, Gochberg DF, Nyman JS, Does MD. Clinically-compatible MRI strategies for discriminating bound and pore water in cortical bone. Magn Reson Med. 2012; 68:1774–84. [PubMed: 22294340]

49. Manhard MK, Horch RA, Harkins KD, Gochberg DF, Nyman JS, Does MD. Validation of quantitative bound- and pore-water imaging in cortical bone. Magn Reson Med. 2014; 71:2166–2171. [PubMed: 23878027]

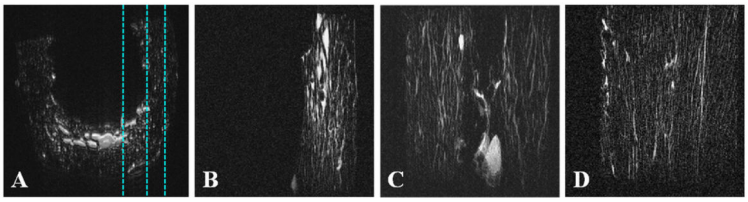

Figure 1.

Axial (A) and three representative sagittal (B, C, D) 2D FSE images of a bone sample. Cortical bone structure is well depicted, with fine structures corresponding to free water residing in the Haversian system of cortical bone.

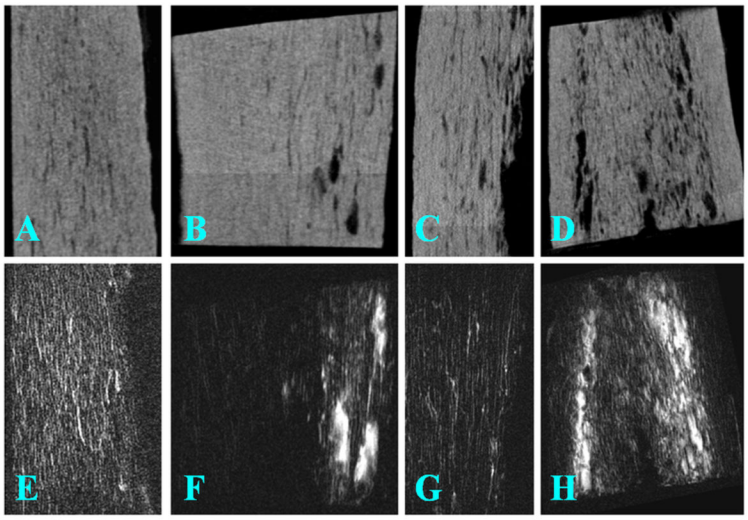

Figure 2.

μCT (top row; A-D) and FSE (bottom row; E-H) imaging of four selected human cortical bone samples. There is a high morphological correlation between these two imaging modalities: the bright signals in FSE images correspond well with signal voids in μCT images

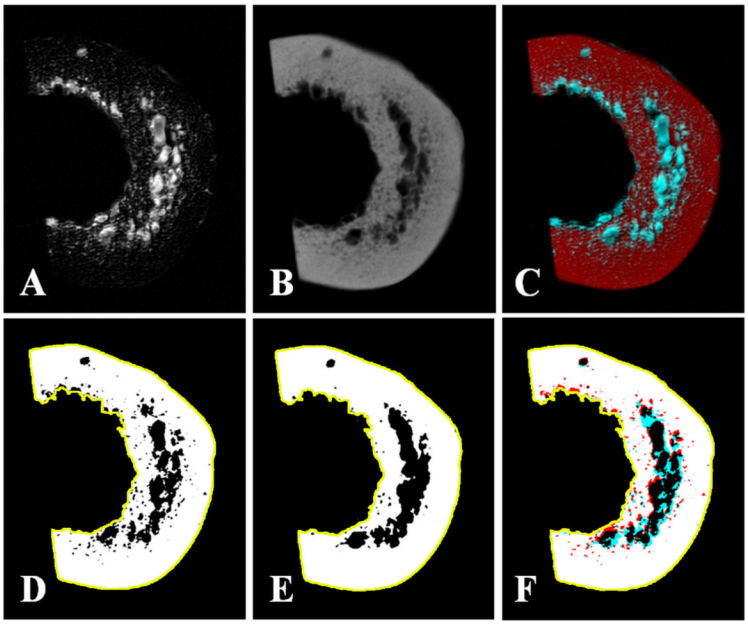

Figure 3.

2D FSE (A) and μCT imaging (B) of a bone sample and the corresponding registered image (C). Regions of interest representing the cortical shell (yellow line, DEF) were drawn, and thresholded. Porosity determined from FSE (D) and μCT (E) were similar, and showed good overlap on the difference image (F), where white, red, and blue areas indicate areas of overlap, μCT-only, and FSE-only, respectively.

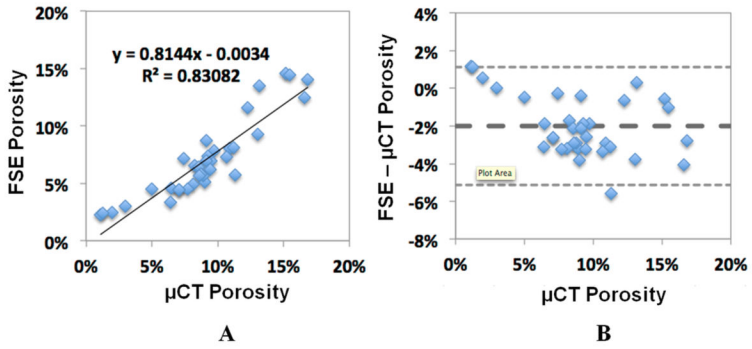

Figure 4.

Linear regression (A) and Bland-Altman analysis (B) were performed between cortical porosity assessed with FSE MRI and µCT imaging. A high correlation between FSE MRI and µCT porosity was observed ($R^2 = 0.83$). Bland-Altman plot shows good agreement between FSE and µCT porosity, with a small bias of -2% for the FSE data and tight limit of agreement at around 3%.

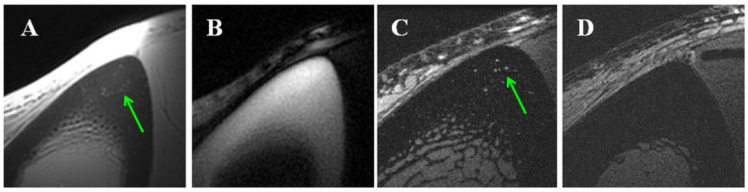

Figure 5.

Axial imaging of the tibia mid-shaft of a 58 year old healthy volunteer with UTE (A), IR-UTE (B) and FSE (C) sequences, and FSE imaging of a 39 year old healthy volunteer (D). UTE detects signal from bone but with limited contrast due to much higher signal from the surrounding muscle and bone marrow fat (A). IR-UTE shows high signal and contrast for cortical bone with excellent suppression of signals from the surrounding muscle and bone marrow fat (B). The fine structures in FSE images correspond to the large Haversian canals (C). The younger volunteer shows no structure in cortical bone with the FSE sequence, consistent with bone without larger canals (D).